EDGE ARTICLE

Check for updates

Tailored engineering of primary catalytic sites and secondary coordination spheres in metalloenzyme-mimetic MOF catalysts for boosting efficient CO_2 conversion†

Jiawei Li, ID *[a] Fan Yang,[a] Benling Yu,[a] Zhongke Dai,[a] Shiyuan Wei,[a] Ying Wu,*[bc] Liuqing He,[d] Fa Zhou,[a] Jianhan Huang ID *[a] and You-Nian Liu ID [a]

The fabrication of metalloenzyme-mimetic artificial catalyst is a promising approach to achieve maximum catalytic efficiency, but the rational integration of sophisticatedly optimized primary catalytic sites (PCS) and secondary coordination spheres (SCS) for specific transformation poses a grand challenge. Here in this work, we report the tailored engineering of Cu PCS and perfluoroalkyl SCS onto a zirconium-based framework [UiO-67-(BPY-Cu)-F_x (x = 3, 5, 7, 11)] [BPY = 2,2'-bipyridine-5,5'-dicarboxylate] that can be utilized in the highly efficient carboxylic cyclization reaction between propargylamines and flue gas CO_2. The perfluoroalkyl groups act as tunable SCS that can facilely adjust the surface electronegativity, hydrophobicity, as well as the CO_2 affinity and water vapor-resistance by simply varying the chain length. Meanwhile, the synergy between the Cu PCS and perfluoroalkyl SCS significantly facilitated the cyclization step by stabilizing the critical transition state, leading to the fast cyclization to the oxazolidinone ring. Owing to these features, UiO-67-(BPY-Cu)-F_7 exhibited remarkable metalloenzyme-mimetic catalytic behavior by greatly facilitating the binding of propargylamines and CO_2, promoting the stabilization of the critical transition state to cyclization, and boosting the releasing of oxazolidinones, which have been systematically investigated by the combination of substrate adsorption tests, *in situ* Fourier transform infrared spectra, grand canonical Monte Carlo simulations, density functional theory calculations, *etc.* Consequently, UiO-67-(BPY-Cu)-F_7 showed outstanding catalytic performance in the carboxylic cyclization of propargylamines and flue gas CO_2 under ambient conditions, exhibiting 64 times higher turnover frequency (TOF) than that of homogeneous or other MOF catalysts, and exhibiting the highest TOF under similar conditions. The present work not only provides an alternative strategy for the construction of advanced carboxylic cyclization systems, but also paves a new direction in the development of CO_2 conversion with exceptional activity through the tailored engineering of PCS and SCS in metalloenzyme-mimetic artificial catalysts.

Introduction

As the primary greenhouse gas contributing to climate change, the escalating levels of carbon dioxide (CO_2) emission present formidable environment challenges on a global scale. In this context, capturing and converting CO_2 into high-value products have emerged as a pivotal frontier in the realm of sustainable chemistry.[1] The carboxylic cyclization of propargylamine and CO_2 serves as a facile pathway for the preparation of 2-oxazolidinones,[2] a N-containing heterocyclic compound with widespread applications in antibacterial drugs, monoamine oxidase inhibitors, *etc.*, which have a global market of billions of dollars annually.[3] From the perspectives of economy and ecology, the utilization of low-cost catalysts such as non-noble-metals and CO_2 directly from flue gas under ambient conditions is highly favorable, but the inherent inertness of both the non-noble-metal and low-concentration CO_2 in flue gas led to largely compromised efficiency.[4] This paradox between economy, ecology and efficiency unambiguously underlines the most critical challenge in advancing towards a more practical CO_2 conversion paradigm.

[a]College of Chemistry and Chemical Engineering, Hunan Provincial Key Laboratory of Micro and Nano Material Interface Science, Central South University, Changsha 410083, Hunan, P. R. China. E-mail: lijiawei@csu.edu.cn; jianhanhuang@csu.edu.cn

[b]GuangDong Engineering Technology Research Center of Modern Fine Chemical Engineering, School of Chemical Engineering and Light Industry, Guangdong University of Technology, Guangzhou 510006, P. R. China

[c]School of Chemistry and Chemical Engineering, South China University of Technology, Guangzhou, Guangdong, 510641, P. R. China. E-mail: yingwu@gdut.edu.cn

[d]The Second Xiangya Hospital of Central South University, Changsha 410000, Hunan, P. R. China
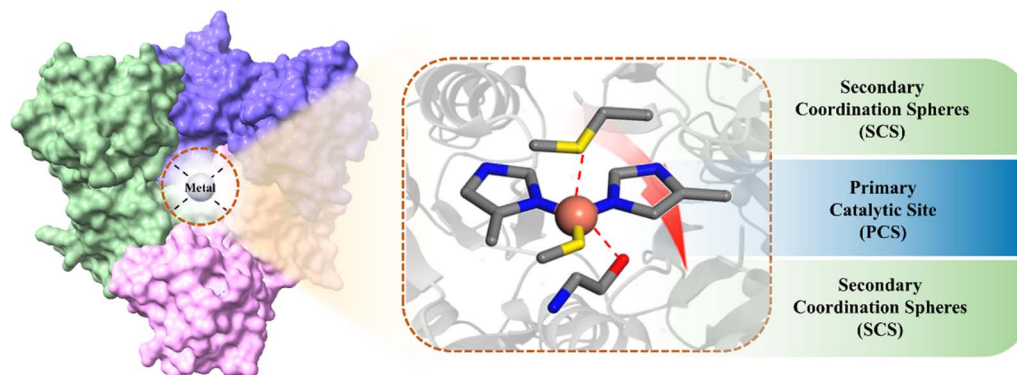
† Electronic supplementary information (ESI) available. See DOI: https://doi.org/10.1039/d5sc01004g

Metalloenzymes, as the most powerful catalysts towards specific biochemical transformation, offer unique insights from nature to the fabrication of advanced CO_2-converting systems.[5] The exceptional activity of metalloenzymatic catalysis arises from the sophisticatedly optimized primary catalytic sites (PCS) and secondary coordination spheres (SCS) within a metalloenzyme, which supports highly cooperative substrate binding, confined catalysis, and product releasing processes (Scheme 1a).[6] Generally, the PCS are composed of non-noble-metals and an inner coordination sphere to drive the biochemical catalysis, while the SCS play an essential role in facilitating substrate binding, stabilizing the transition state and conformational structure, and promoting the release of products.[7] Therefore, the key fundamental principle to fabricate a highly efficient metalloenzyme-mimetic artificial catalyst is the construction of catalytic pockets with judiciously engineered PCS and SCS, where the entire structure can proceed in a concerted manner to emulate the essential features of a metalloenzyme. In this context, metal–organic-frameworks (MOFs) as a highly porous, versatile a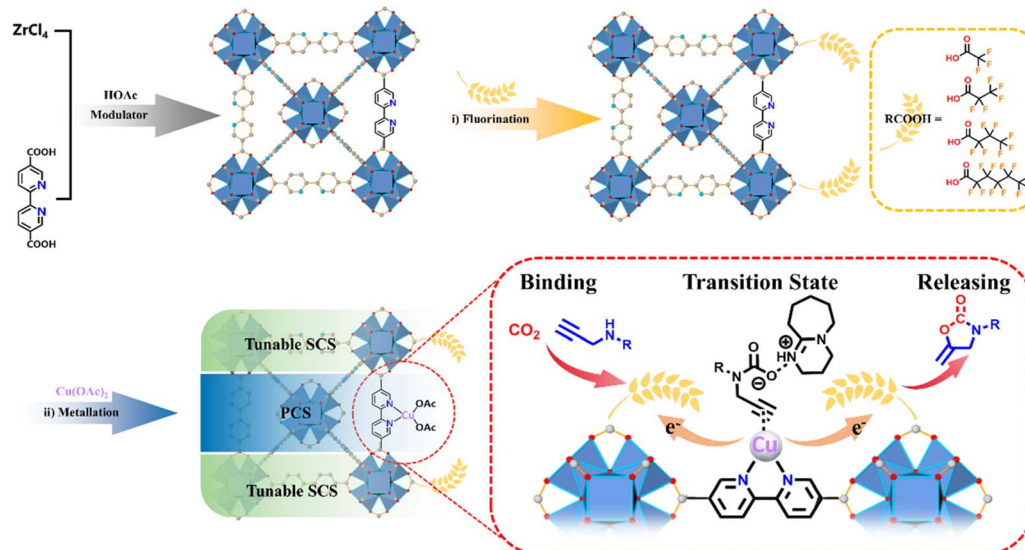nd tunable platform should be an ideal selection by rationally incorporating essential metal active sites and an appropriate surrounding microenvironment.[8]

Here we attempted the tailored engineering of PCS and SCS in MOF catalysts for the development of a metalloenzyme-mimetic carboxylic cyclization process by a systematic evaluation of the molecular properties. Firstly, for the substrate propargylamine, whose skeleton consists of both hydrophobic alkynyl and hydrophilic –NH groups, an appropriate surface hydrophobicity of SCS is necessary for the favorable binding of propargylamine. For the other substrate flue gas CO_2, which is always accompanied by dilute CO_2 and water vapor,[9] excellent CO_2-philicity, as well as superior H_2O-resistance properties are indispensable for maintaining long-term activity and stability. Secondly, the charge distributions of the product oxazolidinone skeletons were investigated by density functional theory (DFT) calculations. By using N-methyl propargylic amine (**1a**) and the corresponding 2-oxazolidinone (**2a**) as the basic model substances, the simulation results showed that **2a** is overall more electronegative than **1a**, suggesting that prominent electronegative SCS may be conducive to the efficient release of

Scheme 1 (a) PCS and SCS in a natural metalloenzyme. (b) Synthetic scheme of [UiO-67-(BPY-Cu)-F$_x$ (x = 3, 5, 7, 11)].

oxazolidinone. Additionally, the metal catalyst has been proved to promote the cyclization to oxazolidinone through stepwise charge transfer processes.[1b] Thus, the rational regulation of the electronic state of PCS through the synergy with SCS might be reasonable for improving its intrinsic activity.

Bearing these in mind, we report the fabrication of metalloenzyme-mimetic noble-metal-free MOF catalysts [UiO-67-(BPY-Cu)-F_x ($x = 3, 5, 7, 11$)] for the highly efficient carboxylic cyclization reaction between propargylamine and flue gas CO_2 (Scheme 1b). Through the tailored engineering of Cu as the PCS and perfluoroalkyl as tunable SCS onto the framework, UiO-67-(BPY-Cu)-F_7 exhibited remarkable metalloenzyme-mimetic catalytic behavior by greatly facilitating the binding of propargylamines and CO_2, boosting the confined catalytic reaction, and promoting the release of oxazolidinones, which leads to a 64 times higher turnover frequency (TOF) than that of homogeneous or other MOF catalysts, and exhibiting the highest TOF in a non-noble-metal-catalyzed carboxylic cyclization reaction under ambient conditions.

Results and discussion

Synthesis and characterization of MOF catalysts

UiO-67-BPY was prepared according to the reported method.[10] As illustrated in Scheme 1b, UiO-67-BPY was initially synthesized by the combination of $ZrCl_4$ and BPY in DMF at 120 °C for 24 hours, utilizing HOAc as the modulator. The resulting UiO-67-BPY exhibited a highly crystalline structure, as evidenced by the powder X-ray diffraction (PXRD) pattern, which matched well with the simulated one (Fig. 1a). The N_2 adsorption–desorption isotherms at 77 K revealed a reversible type I microporous adsorption isotherm according to the IUPAC classification, with a calculated BET surface area of 2369 m^2 g^{-1} (Fig. 1b). Scanning electron microscopy (SEM) images depicted UiO-67-BPY as regular and uniform octahedral morphology, with a diameter of 1 μm (Fig. S1†). It is noteworthy that the treatment of excess modulator in the synthesis of UiO series MOFs usually leads to a residual modulator coordinated in the Zr-clusters, which could be further exchanged by other functional groups.[11] To identify the quantity of the residual HOAc in UiO-67-BPY, ^{1}H NMR analysis of the digested UiO-67-BPY was first conducted, indicating a BPY/HOAc ratio of 1 : 0.38 (Fig. 1c). Thus, the molecular formula of the defective UiO-67-BPY can be derived as $Zr_6O_4(OH)_4(BPY)_{5.04}(OAc)_{1.91}$. To further verify the molecular formula of the defective UiO-67-BPY, thermogravimetry analysis was conducted. As shown in Fig. 1d, the first weight loss (4.95%) from 30 to 100 °C corresponds to the removal of adsorbed solvents in the MOF. The second weight loss (62.77%) from 100–800 °C corresponds to decomposition of UiO-67-BPY to $6ZrO_2$ (739.34 g mol^{-1}), consistent with a weight loss of 63.39% based on the conversion of $Zr_6O_4(OH)_4(BPY)_{5.04}(OAc)_{1.91}$ to $6ZrO_2$.

After determining the exact quantity of the defects, we attempted the direct binding of perfluoroalkyl carboxylic acids with the unsaturated Zr_6-clusters. The UiO-67-BPY crystals were immersed in the solutions of perfluoroalkyl carboxylic acids with varying chain lengths ($C_nF_{2n+1}COOR$, $n = 1, 2, 3, 5$) in DMF at room temperature for 24 hours, resulting in the formation of
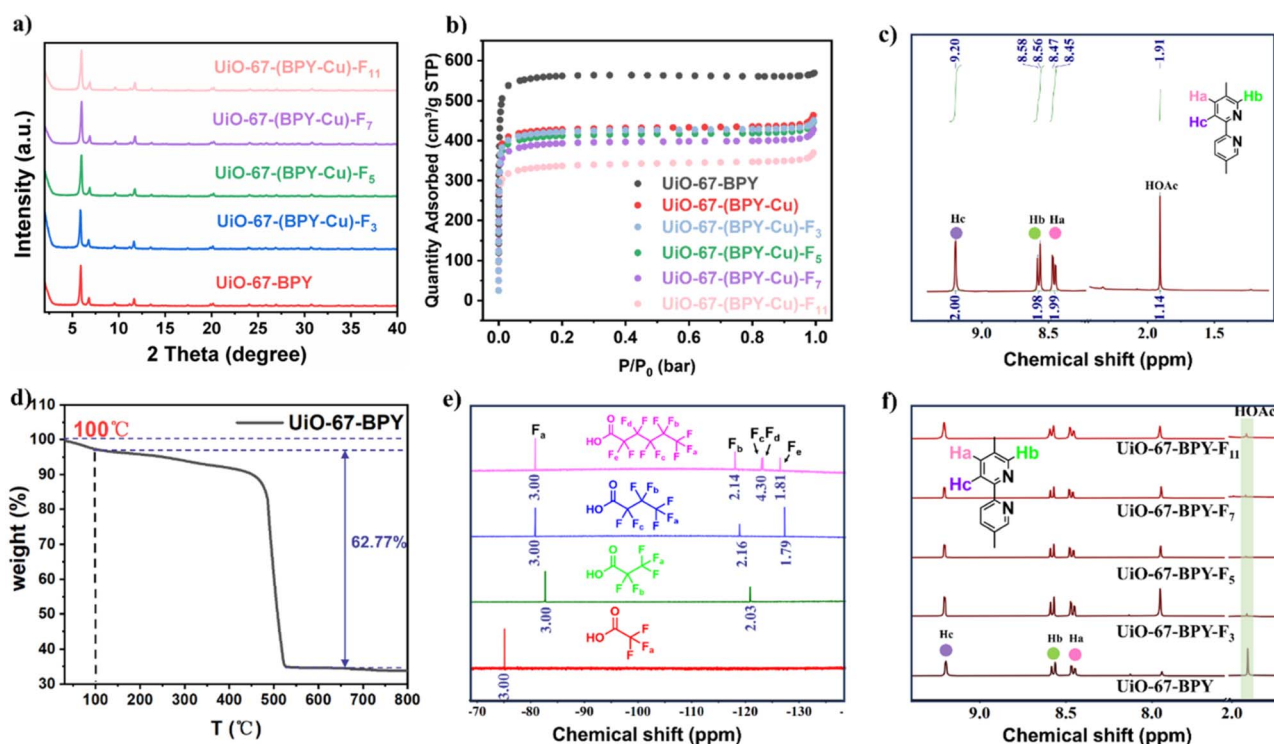

Fig. 1 (a) PXRD patterns of different UiO MOFs. (b) N_2 adsorption and desorption isotherms of different UiO MOFs. (c) ^{1}H NMR spectroscopy of digested defective UiO-67 MOFs. (d) TG of UiO-67-BPY. (e) ^{19}F NMR and (f) ^{1}H NMR spectroscopy of digested UiO-67-BPY-F_x ($x = 3, 5, 7, 11$).

UiO-67-BPY-F$_x$ (x = 3, 5, 7, 11). The successful fluorination was first confirmed using the ^{19}F NMR spectra of the acid-digested samples of UiO-67-BPY-F$_x$, which clearly showed the characteristic peaks of different perfluoroalkyl chains (Fig. 1e). Meanwhile, ^{1}H NMR analysis of the digested UiO-67-BPY-F$_x$ showed that the peaks corresponding to HOAc almost disappeared (Fig. 1f), indicating the complete substitution of the regulator HOAc by the perfluoroalkyl groups. Moreover, the water contact angle tests manifested a notable increase with the elongation of the length of perfluoroalkyl chains, increasing from 75° for UiO-67-BPY to 140° for UiO-67-BPY-F$_{11}$ (Fig. S2†). These results demonstrated the successful transformation of the surface microenvironment from hydrophilic to hydrophobic by the incorporation of perfluoroalkyl chains.

Finally, the post-synthetic metalation of UiO-67-BPY-F$_x$ with Cu(OAc)$_2$·H$_2$O was carried out in acetonitrile at room temperature for 24 hours to afford UiO-67-(BPY-Cu)-F$_x$ (x = 3, 5, 7, 11). The integrity of the MOF structures after the metalation was confirmed using the PXRD patterns (Fig. 1a). The N$_2$ adsorption results at 77 K indicated a decrease in the adsorption amounts and S$_{BET}$ of UiO-67-(BPY-Cu)-F$_x$, as a result of the pore space occupation by perfluoroalkyl chains and metal species (Fig. 1b). The TEM and elemental mapping images displayed a uniform distribution of Cu over the block crystals (Fig. 2i). Inductively coupled plasma mass spectrometry (ICP-MS) indicated that the Cu content in the UiO-67-(BPY- Cu)-F$_x$ was about 10.5 wt%. To ascertain the valence state and coordination modes of the Cu species in the metallized MOFs, X-ray photoelectron spectroscopy (XPS) analyses were conducted. As shown in Fig. 2g, the binding energy (BE) of the N 1s peak at 398.2 eV can be ascribed to the N atoms in the free BPY ligand, while the BE of the N atom at 399.2 eV is attributed to the BPY-Cu species for UiO-67-(BPY-Cu)-F$_7$,[12] verifying the successful coordination of Cu(OAc)$_2$ to the framework. In addition, the characteristic peaks of BEs of Cu
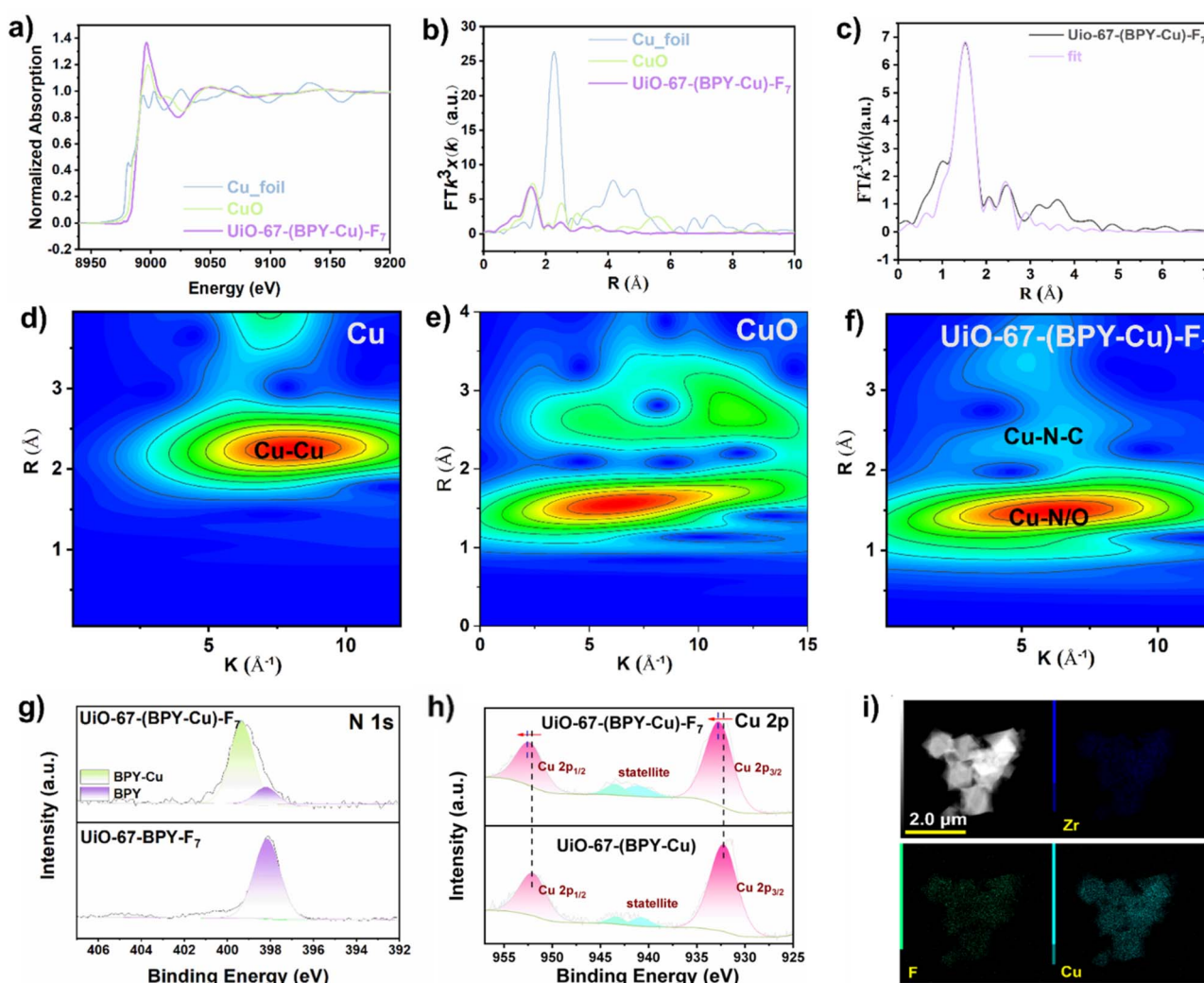

Fig. 2 (a) XANES in R space at the Cu K-edge adsorption of Cu foil (blue), Cu$_2$O, and UiO-67-(BPY-Cu)-F$_7$. (b) EXAFS in R space at the Cu K-edge adsorption of Cu foil (blue), Cu$_2$O, and UiO-67-(BPY-Cu)-F$_7$. (c) EXAFS in R space at the Cu K-edge adsorption of UiO-67-(BPY-Cu)-F$_7$ and the fitted curve. (d–f) The wavelet transform curves of Cu foil, CuO and UiO-67-(BPY-Cu)-F$_7$. (g) XPS spectra of UiO-67-BPY-F$_7$ and UiO-67-(BPY-Cu)-F$_7$ in the N 1s region. (h) XPS spectra of UiO-67-(BPY-Cu) and UiO-67-(BPY-Cu)-F$_7$ in the Cu 2p region. (i) TEM-elemental mapping of UiO-67-(BPY-Cu)-F$_7$.

$2p^{3/2}$ at 934 eV and Cu $2p^{1/2}$ at 945 eV, as well as the satellite peaks, both suggest that the oxidation state of Cu is +2 in UiO-67-(BPY-Cu)-F_x (Fig. 2h).[13] It is noteworthy that the peaks of BEs of Cu in UiO-67-(BPY-Cu) shifted to lower positions than that in UiO-67-(BPY-Cu)-F_7, suggesting the electron-withdrawing effect of perfluoroalkyl groups on Cu centers. Moreover, we calculated the charge density difference of Cu in UiO-67-(BPY-Cu) and UiO-67-(BPY-Cu)-F_7, which indicated that after the decoration of perfluoroalkyl, the Cu centers mainly lose electrons, and the positive electric field is more significant in UiO-67-(BPY-Cu)-F_7 (Fig. S4†). The above results verified the apparent interactions between the Cu PCS and perfluoroalkyl SCS in UiO-67-(BPY-Cu)-F_7.

To further determine the coordination environments and oxidation states of Cu in UiO-67-(BPY-Cu)-F_7, X-ray absorption fine structure (XAFS) was carried out. X-ray absorption near-edge structure (XANES) spectroscopy of different standard samples confirmed the Cu^{II} oxidation state in UiO-67-(BPY-Cu)-F_7 (Fig. 2a). Fitting of the extended X-ray absorption fine structure (EXAFS) data for UiO-67-(BPY-Cu)-F_7 at the Cu K-edge manifests that the coordination number of Cu is about 4, suggesting the coordination to two N atoms from BPY and two O atoms from two OAc- groups with the average Cu–N/O bond length of 1.98 Å (Fig. 2b, Table S1†). The wavelet-transform EXAFS analysis further supported that the Cu coordination bond length parameters in UiO-67-(BPY-Cu)-F_7 ($k = 5.4$ Å, $r = 1.5$ Å) were comparable to those observed in CuO ($k = 5.5$ Å, $r = 1.6$ Å) rather than Cu foil ($k = 7.8$ Å, $r = 2.3$ Å), demonstrating the presence of Cu–N/O bonds in these structures (Fig. 2d–f). The above results clearly confirmed the successful construction of UiO-67-(BPY-Cu)-F_x.

Catalytic performances in the cyclization reaction

With the well-prepared UiO-67-(BPY-Cu)-F_x in hand, we started to examine their catalytic performances in the carboxylic cyclization of propargylamine and CO_2. Initially, the reaction between **1a** and CO_2 in the presence of Cu(OAc)$_2$ (5 mol%) at 25 °C gave the corresponding product with a yield of only 17% (Table 1, entry 2). Similarly, when 1,8-diazabicyclo [5,4,0] undecene-7 (DBU) (25 mol%) was used alone, the yield of the product was 22% (Table 1, entry 1). By using the mixture of Cu(OAc)$_2$ (5 mol%) and DBU (25 mol%) as the co-catalyst, the product yield elevated to 52% (Table 1, entry 3). Upon employing UiO-67-(BPY-Cu) (5 mol% Cu) as the catalyst, a further increase of the yield to 67% can be observed (Table 1, entry 4). Impressively, the introduction of perfluoroalkyl groups on the framework gave greatly increased catalytic efficiency. For example, incorporating a short perfluoroalkyl (F_3) group can give the product with a yield of 66% with largely reduced Cu loading (0.5 mol%) (Table 1, entry 5). When the length of the perfluoroalkyl chain was extended from F_5 to F_7, an optimal yield of 99% and a remarkably elevated TOF value of 49.5 can be achieved (Table 1, entries 6 and 7), which is 19 and 15 times higher than that of the homogeneous counterpart and the unfluorinated MOF, respectively, and is among the highest TOF in non-noble-metal-catalyzed carboxylic cyclization reactions under similar conditions (Table S2†). Further extending the perfluoroalkyl chain to F_{11} led to a slight decline in the activity, possibly due to the pore size limitation and mass transfer hindrance (Table 1, entry 8). These findings showed the prominent impact of the perfluoroalkyl decoration on the catalytic performance.

Table 1 Evaluation of different reaction parameters for carboxylic cyclization between **1a** and $CO_2{}^a$

Entry	Catalyst	CO_2	Yield[b] (%)	TON[c]	TOF[d] (h⁻¹)
1	—	Pure	22%	—	—
2[e]	Cu(OAc)$_2$	Pure	17%	3.4	0.85
3[f]	Cu(OAc)$_2$	Pure	52%	10.4	2.6
4[f]	UiO-67-(BPY-Cu)	Pure	67%	13.4	3.35
5	UiO-67-(BPY-Cu)-F_3	Pure	66%	132	33
6	UiO-67-(BPY-Cu)-F_5	Pure	88%	176	44
7	UiO-67-(BPY-Cu)-F_7	Pure	99%	198	49.5
8	UiO-67-(BPY-Cu)-F_{11}	Pure	93%	186	46.5
9[f]	UiO-67-(BPY-Cu)	CO_2 (15%)	35%	7	0.78
10	UiO-67-(BPY-Cu)-F_7	CO_2 (15%)	91%	182	20.22
11[f]	UiO-67-(BPY-Cu)	CO_2 (15%)[g]	15%	3	0.33
12	UiO-67-(BPY-Cu)-F_7	CO_2 (15%)[g]	95%	190	21.11
13	UiO-67-(BPY-Cu)-F_7	Flue gas[h]	91%	182	20.22
14[i]	UiO-67-(BPY-Cu)-F_7	Flue gas[h]	90%	180	20

[a] Reaction conditions: **1a** (1 mmol), CH$_3$CN (2 ml), DBU (0.25 mmol), catalyst (0.5 mol% Cu), 25 °C, 4 h (pure CO_2) or 9 h (15% CO_2). [b] Yields are determined by NMR with trimethylbenzene as the internal standard. [c] TON: moles of product/catalyst. [d] TOF: TON per t. [e] 5 mol% Cu and without DBU. [f] 5 mol% Cu. [g] Catalyst was exposed to humid conditions (RH: 70%) for 12 h before the reaction. [h] N$_2$: 80.5%, CO_2: 15%, O$_2$: 4%, SO$_2$: 0.5%. [i] Fifth catalytic cycle.

This discrepancy in the activity becomes more pronounced when diluted CO_2 ($CO_2 : N_2 = 15 : 85$) was utilized in the catalytic reaction. When UiO-67-(BPY-Cu) (5 mol% Cu) was employed as the catalyst, an obvious reduced yield of 35% was observed in the diluted CO_2 atmosphere (Table 1, entry 9). In stark contrast, UiO-67-(BPY-Cu)-F_7 (0.5 mol% Cu) still exhibited outstanding catalytic performance under the same reaction conditions, emphasizing its proficiency in the adsorption and conversion of dilute CO_2 (Table 1, entry 10). In order to further assess the catalyst's performance under conditions mimicking a real industrial setting, we first conducted the catalytic reaction with diluted CO_2 in a humid environment. This choice stems from the fact that industrial flue gas typically contains considerable amount of water vapor. Impressively, the results turned out that UiO-67-(BPY-Cu) can only give a yield of 15% (Table 1, entry 11), while the existence of water vapor exerts no influence on the reactivity of UiO-67-(BPY-Cu)-F_7 under identical reaction conditions (Table 1, entry 12), exhibiting a significant 64 times higher TOF value. This dominant contrast in activity can be attributed to their distinct difference in the hydrothermal stability. As illustrated in Fig. 3a, the water vapor adsorption amount of UiO-67-(BPY-Cu)-F_7 significantly decreased compared to its unfluorinated counterpart, highlighting its superior resistance towards water vapor. Furthermore, PXRD measurement revealed that UiO-67-(BPY-Cu)-F_7 still retained its framework integrity after exposure to water vapor treatment, while the diffraction peak of UiO-67-(BPY-Cu) totally

disappeared, indicating the decomposition of the framework (Fig. S6†). Moreover, by utilizing a more complex flue gas (N_2: 80.5%, CO_2: 15%, O_2: 4%, SO_2: 0.5%), UiO-67-(BPY-Cu)-F_7 still exhibited a high yield of 91% in the carboxylic cyclization, and could be reused for five times without apparent loss of activity, highlighting its potential application under practical flue gas conditions (Table 1, entries 13 and 14). The combination of PXRD, N_2 adsorption and XPS characterization studies of UiO-67-(BPY-Cu)-F_7 after the catalysis was conducted, showing that the crystallinity, porosity and the Cu active sites are well retained after the carboxylic cyclization test (Fig. S7–S9†). These findings underlined the pivotal role played by perfluoroalkyl decoration in imparting superior stability to the MOF catalyst, thereby preserving its structural integrity and catalytic efficacy under the challenging conditions of practical flue gas environment. These results are particularly crucial in the context of evaluating the catalyst's adaptability and efficiency in real-world scenarios.

Under the optimized reaction conditions, we then evaluated the catalytic activity of the catalyst towards different substrates, and the outcomes are summarized in Table S3.† In the presence of UiO-67-(BPY-Cu)-F_7 and a pure CO_2 atmosphere, diverse propargylamine compounds with different substituents can lead to the corresponding 2-oxazolidinone products with excellent activity. For example, different propargylamines bearing aliphatic groups **2a–c** (-CH_3, *n*-Bu, and *n*-Hex) can be well tolerated in this catalytic system. Meanwhile, benzyl
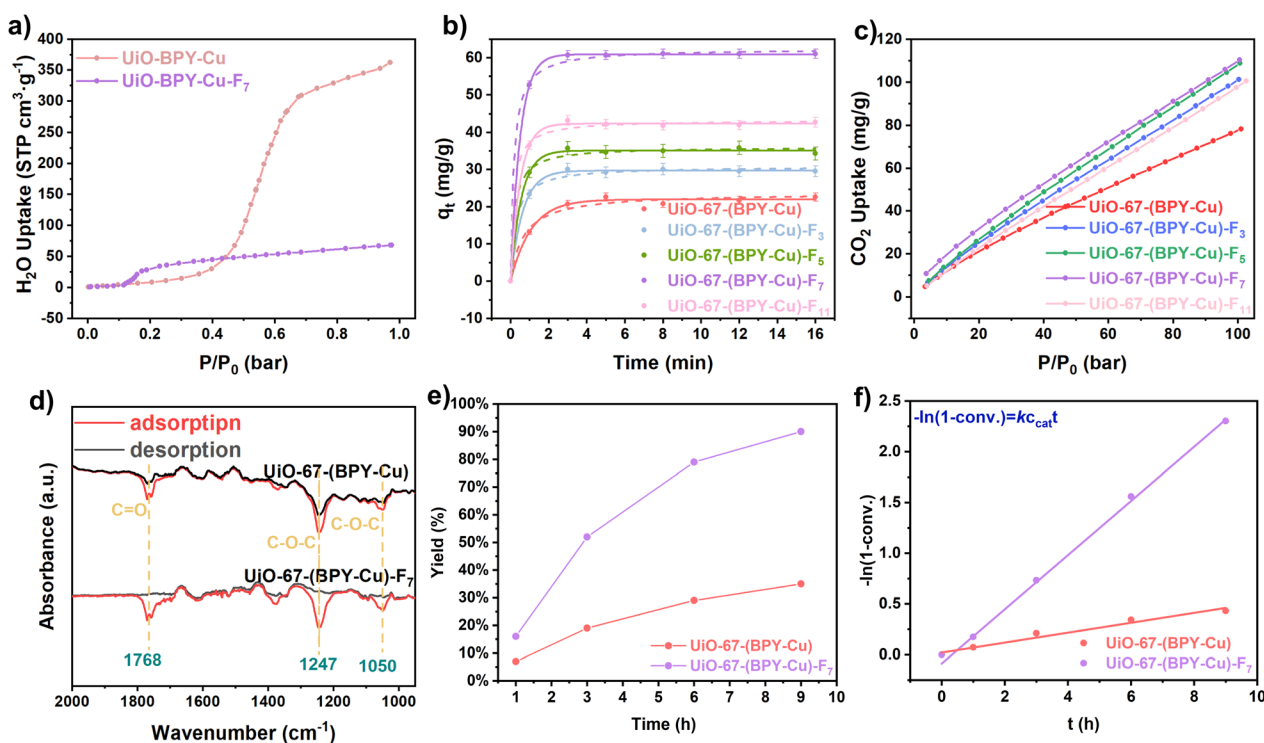

Fig. 3 (a) Water vapor adsorption tests at 298 K of UiO-(BPY-Cu) and UiO-(BPY-Cu)-F_7. (b) **1a** adsorption kinetics of different UiO MOFs. (c) CO_2 adsorption tests at 273 K of UiO-67-(BPY-Cu)-F_x (x = 3, 5, 7, 11) (d) *In situ* FT–IR spectra (red: the adsorption of **2a** at room temperature for 30 min over UiO-(BPY-Cu) and UiO-(BPY-Cu)-F_7; black: further purging with N_2 until there was no change in the band intensity). (e) Plot of the yields of catalytic products *vs.* reaction time in a dilute CO_2 atmosphere. (f) A kinetics study of the carboxylation cyclization reaction between **1a** and dilute CO_2.

propargylamines bearing both electron-donating (OMe, Me) and electron-withdrawing (F, Cl, and CF$_3$) groups **2d–i** can convert to the corresponding oxazolidinones smoothly. It is noteworthy that these reactions also proceeded efficiently when using low-concentration CO$_2$ under humid conditions, with no significant loss of activity. These results highlighted the wide applicability of UiO-67-(BPY-Cu)-F$_7$ in the carboxylic cyclization reaction between propargylamine and flue gas CO$_2$.

Investigation of the metalloenzyme-mimetic catalytic mechanism

In pursuit of unraveling the metalloenzyme-mimetic catalytic process of UiO-67-(BPY-Cu)-F$_x$ in the carboxylic cyclization reaction, we conducted an in-depth mechanism investigation combining several experiments and theoretical calculations. Initially, the substrate binding processes of different catalytic systems were evaluated. For propargylamine, its affinity performance on UiO-67-(BPY-Cu)-F$_x$ was first examined by contact angle experiments using **1a** as the model substance. The results showed that **1a** exhibited excellent affinity towards all these perfluoroalkyl-decorated MOF catalysts with contact angles ranging from 10–16° (Fig. S10†). Then, we further investigated the adsorption kinetics of propargylamine to distinguish the binding behaviors of the different catalysts. Among the various MOFs tested, UiO-67-(BPY-Cu)-F$_7$ exhibited

discernibly superior enrichment and adsorption behaviors of **1a**, probably owing to its most appropriate surface hydrophobicity and electronegativity (Fig. 3b and 4a). For the other substrate CO$_2$, the adsorption and desorption isotherms were measured at 0 °C (~273 K) and 25 °C (~298 K) for all obtained MOFs (Fig. 3c and S11†). A comparison of the isotherms between UiO-67-BPY and UiO-67-(BPY-Cu)-F$_x$ indicated increased CO$_2$ uptake with the inclusion of the perfluoroalkyl chains. This phenomenon is attributed to the interaction of C–F dipoles with the quadrupole of CO$_2$, rendering preferential positioning of CO$_2$ molecules around the perfluoroalkyl groups within the framework, as verified by DFT calculations (Fig. 4b). The isosteric heat of adsorption (Q_{st}) ranged from 13.9 to 32.6 kJ mol^{-1} for these MOFs, lower than that of chemical adsorption (41.7–84.0 kJ mol^{-1}) (Fig. S12†). The above results clearly suggested the remarkable effect of the SCS on the efficient binding of both propargylamine and CO$_2$.

Next, in situ FT-IR spectra were recorded for UiO-67-(BPY-Cu) and UiO-67-(BPY-Cu)-F$_7$ to study their desorption behavior of 2-oxazolidinones (**2a**), which helps to shed light on the product releasing process. As shown in Fig. 3d, an obvious characteristic stretching vibration band of the C=O bond at 1768 cm^{-1} and the asymmetric and symmetric stretching vibration bands of the C–O bond at around 1247 and 1050 cm^{-1} assignable to **2a** were similarly observed for both UiO-67-(BPY-Cu) and UiO-67-(BPY-Cu)-F$_7$ after the adsorption of **2a**. However, after further
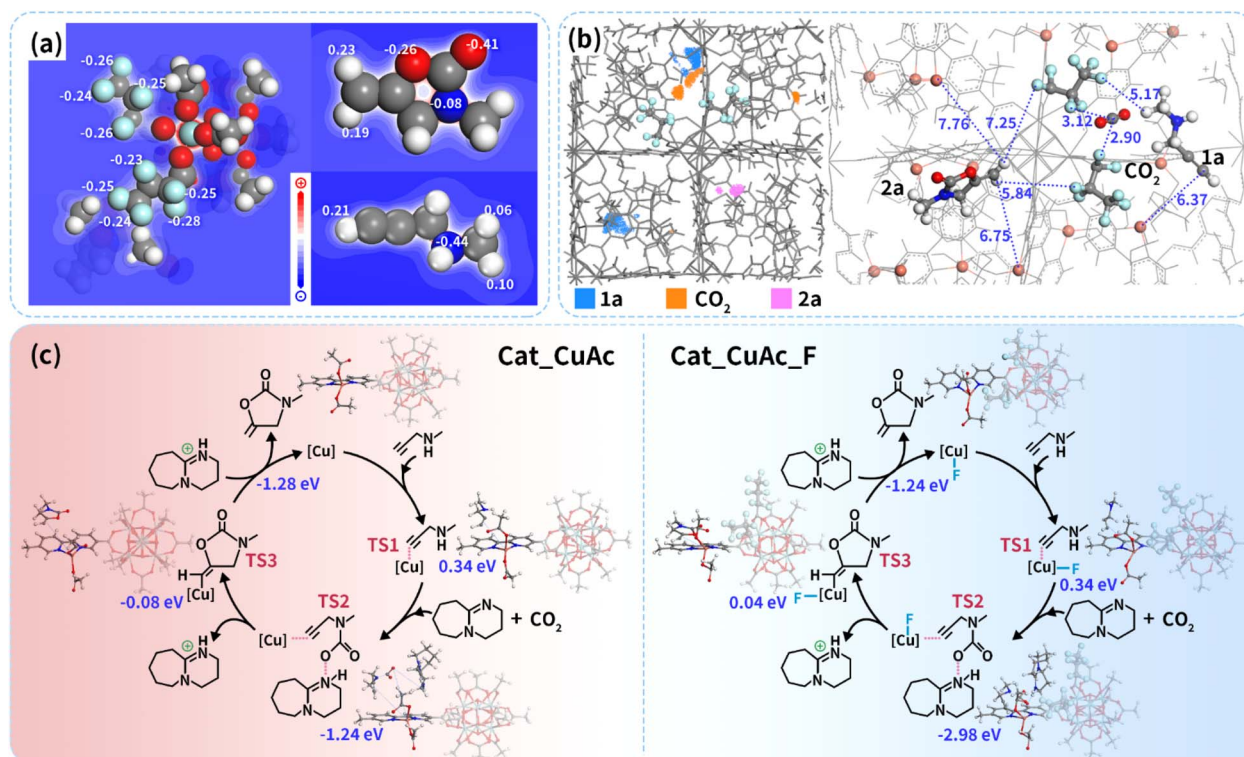

Fig. 4 (a) Atomic charges of **1a**, **2a** and **Cat_CuAc_F**, with the electrostatic potential field illustrated. (b) Competitive adsorption configurations of **1a**, **2a** and CO$_2$ in the framework of **Cat_CuAc_F**, the adsorption density distribution of the guests is colored as blue, pink and orange for **1a**, **2a** and CO$_2$, respectively; the distance between the guests and the catalyst is labeled in the unit of angstrom. Atom color code: carbon = grey, hydrogen = white, oxygen = red, nitrogen = navy, fluorine = cyan, copper = coral. (c) The catalysis mechanism of **Cat_CuAc** and **Cat_CuAc_F**, with the configuration of each TS step and the corresponding energy barrier.

purging the samples with N_2, the characteristic peaks of **2a** at 1768, 1247 and 1050 cm^{-1} almost vanished in UiO-67-(BPY-Cu)-F$_7$, while the adsorption of **2a** was still apparently detectable in UiO-67-(BPY-Cu). These results implied the obvious weaker adsorption interaction between **2a** and UiO-67-(BPY-Cu)-F$_7$, which can be ascribed to the repulsive effect by the electronegative pore structure of the MOF and the skeleton of **2a**. Indeed, our grand canonical Monte Carlo simulation results indicated that UiO-67-(BPY-Cu)-F$_7$ preferentially interacts with the reactant **1a** and CO_2 rather than the product **2a**, where **1a** and CO_2 molecules stabilize closer together due to the attraction effects of F$_7$ chains, with the C (CO_2)–F and H (**1a**)–F distance of 3.12 Å and 5.17 Å, respectively, compared to the H (**2a**)–F distance of 5.84–7.25 Å (Fig. 4b). This competitive adsorption behavior may be attributed to the different electrostatic nature of **1a** and **2a**. As illustrated in Fig. 4a, compared to the negative charges of oxygen atoms (-0.41 to -0.26 e) in **2a**, the relatively positive charges of H atoms (0.06–0.21 e) in **1a** allow the molecule to be thermodynamically more favorable towards F atoms with negative charges (about -0.25 e). This feature was significantly beneficial to the desorption of **2a** from the surface of UiO-67-(BPY-Cu)-F$_7$, thereby promoting the product unleashing process.

Subsequently, we elucidated the confined catalytic process by DFT calculations. We utilized the BPY-Cu(OAc)$_2$ moiety and the adjacent Zr$_6$ cluster in both UiO-67-(BPY-Cu)-F$_7$ (**Cat_-CuAc_F**) and UiO-67-(BPY-Cu) (**Cat_CuAc**) as the simulation models to clarify the synergy of the Cu PCS and the perfluoroalkyl SCS. Owing to the favorable substrate binding properties of UiO-67-(BPY-Cu)-F$_7$, propargylamine **1a** and CO_2 were preferentially adsorbed and accumulated on the catalyst's surface. Then, the C≡C in **1a** was activated through the coordination to Cu. Subsequently, –NH group in **1a** undergoes electrophilic attack by CO_2 with the assistance of DBU to produce the critical transition state (**TS2**). Impressively, DFT calculations indicated that the energy barrier of the **TS2** step for **Cat_CuAc_F** is significantly lower compared to that of **Cat_CuAc** (-2.98 *vs.* -1.24 kcal mol^{-1}). This apparent discrepancy results from the much more electron-deficient Cu site in **Cat_CuAc_F** due to the intense electron-withdrawing effect of the perfluoroalkyl group, which facilitates the electron transfer from the alkynyl group to Cu and thus promotes the nucleophilic attack of the negatively charged oxygen atom on the alkynyl. Eventually, cyclization from the **TS2** complex to **TS3** occurred, and the formed intermediate undergoes H transfer to regenerate the base, and give the final product **2a**. Note that the product **2a** can be rapidly released from the catalyst's surface and start another catalytic cycle.

After determining the substrate binding, confined catalytic reaction and product releasing processes of UiO-67-(BPY-Cu)-F$_7$, we further investigated its rate constant to evaluate the reaction kinetics. We first monitored the catalytic yields of UiO-67-(BPY-Cu) and UiO-67-(BPY-Cu)-F$_7$ in the reaction between **1a** and diluted CO_2 over its reaction time. The results showed that UiO-67-(BPY-Cu)-F$_7$ gave apparently overwhelming activity compared to its unfluorinated counterpart (Fig. 3e). Specifically, UiO-67-(BPY-Cu)-F$_7$ exhibited an obviously higher catalytic efficiency from the initiation of the reaction, and quickly reached 91%, while the catalytic rate of UiO-67-(BPY-Cu) was notably slow, ultimately achieving a yield of only 35%. In order to quantitatively evaluate the reactivities of UiO-67-(BPY-Cu) and UiO-67-(BPY-Cu)-F$_7$, their apparent reaction rate constants were calculated. As is evident from Fig. 3f, UiO-67-(BPY-Cu)-F$_7$ ($k = 106.84$ ml h^{-1} mmol$_{Cu}^{-1}$) results in 55 times higher rate than the unfluorinated UiO-67-(BPY-Cu) ($k = 1.96$ ml h^{-1} mmol$_{Cu}^{-1}$), implying that the synergy between the Cu PCS and perfluoroalkyl SCS facilitates greatly enhanced reaction kinetics in the carboxylic cyclization reaction. All the above results unambiguously highlighted the metalloenzyme-mimetic catalytic process of UiO-67-(BPY-Cu)-F$_7$ in the carboxylic cyclization reaction.

Conclusions

In summary, we have reported the tailored engineering of metalloenzyme-mimetic non-noble-metal MOF catalysts by introducing the single-site Cu as the PCS and perfluoroalkyl groups as tunable SCS. The combination of substrate adsorption tests, *in situ* Fourier transform infrared spectra, GCMC simulations and DFT calculations highlighted the remarkable metalloenzyme-mimetic catalytic behavior of UiO-67-(BPY-Cu)-F$_7$ in the carboxylic cyclization reaction by greatly promoting the binding of propargylamines and flue gas CO_2, stabilizing the transition state to cyclization, and facilitating the oxazolidinone release. These metalloenzyme-mimetic features of UiO-67-(BPY-Cu)-F$_x$ led to overwhelming catalytic performance in the carboxylic cyclization reaction, exhibiting the highest TOF in non-noble-metal-catalyzed carboxylic cyclization reactions under ambient conditions. This work proposes an alternative strategy for the construction of advanced carboxylic cyclization catalytic systems for the facile preparation of 2-oxazolidinones. It also offers a promising new insight into the development of highly efficient CO_2 conversion through the tailored engineering of PCS and SCS in metalloenzyme-mimetic artificial catalysts.

Data availability

The data that support the findings of this study are available in the ESI† of this article.

Author contributions

Jiawei Li and Fan Yang contributed the central idea, analyzed most of the data, and wrote the initial draft of the paper. Jianhan Huang acquired of the financial support for the project leading to this publication. The remaining authors contributed to refining the ideas, carrying out additional analyses and finalizing this paper.

Conflicts of interest

There are no conflicts to declare.

Acknowledgements

Notes and references

1 (a) P. D. Luna, C. Hahn, D. Higgins, S. A. Jaffer, T. F. Jaramillo and E. H. Sargent, Science, 2019, 364, eaav3506; (b) C. A. Trickett, A. Helal, B. A. Al-Maythalony, Z. H. Yamani, K. E. Cordova and O. M. Yaghi, Nat. Rev. Mater., 2017, 2, 17045; (c) M. Ding, R. W. Flaig, H.-L. Jiang and O. M. Yaghi, Chem. Soc. Rev., 2019, 48, 2783–2828; (d) G. A. Olah, G. K. S. Prakash and A. Goeppert, J. Am. Chem. Soc., 2011, 133, 12881–12898.

2 (a) X. Yang, L. Xu, Y. Zhu, S. Zhang, G. Jia and J. Du, J. CO$_2$ Util., 2023, 74, 102531; (b) A. Sattar, V. Esmail, S. Marjan, H. Akram and B. Ahmedreza, J. CO$_2$ Util., 2017, 19, 120–129.

3 (a) J. S. Karen and R. B. Michael, Ann. N. Y. Acad. Sci., 2011, 1241, 48–70; (b) D. J. Diekema and R. N. Jones, Lancet, 2001, 358, 1975–1982; (c) Q. Zhao, L. Xin, Y. Liu, C. Liang, J. Li, Y. Jian, H. Li, Z. Shi, H. Liu and W. Cao, J. Med. Chem., 2021, 64, 10557–10580.

4 (a) H.-N. Qin, M.-W. He, J. Wang, H.-Y. Li, Z.-Y. Wang, S.-Q. Zang and C. W. M. Thomas, J. Am. Chem. Soc., 2024, 146, 3545–3552; (b) W. Wang, T. Wang, S. Chen, Y. Lv, L. Salmon, B. Espuche, S. Moya, O. Morozova, Y. Yun, D. D. Silvio, N. Daro, M. Berlande, P. Hapiot, J.-L. Pozzo, H. Yu, J.-R. Hamon and D. Astruc, Angew. Chem., Int. Ed., 2024, e202407430; (c) X. Chen, J.-Y. Song, J. Zheng, Y.-M. Wang, J. Luo, P. Weng, B.-C. Cai, X.-C. Lin, G.-H. Ning and D. Li, J. Am. Chem. Soc., 2024, 146, 19271–19278; (d) Z.-W. Zheng, J.-J. Zhou, H. Liu, X.-Y. Zhang, J. Zhao, D.-S. Zheng, K. Huang and D.-B. Qin, Inorg. Chem., 2024, 63, 16878–16887; (e) J. Qiu, X. Qi, K. Zhu, Y. Zhao, H. Wang, Z. Li, H. Wang, Y. Zhao and J. Wang, Green Chem., 2024, 26, 6172–6179; (f) Z. Zhang, K. Shen, Q. Zhang, C. Duan and X. Jing, Dalton Trans., 2024, 53, 10060–10064; (g) Q. Cao, W. Sun, Z. Xiao, X. Zhou, L. Lu, H. Hou, Y. Chen and L. Wang, Small, 2024, 20, 2404202; (h) V. Parihar, G. Singh, N. Duhan, S. Kumar, T. J. D. Kumar and C. M. Nagaraja, ChemSusChem, 2024, e202401497; (i) A.-L. Gu, Y.-X. Zhang, Z.-L. Wu, H.-Y. Cui, T.-D. Hu and B. Zhao, Angew. Chem., Int. Ed., 2024, e202114817; (j) C.-S. Cao, S.-M. Xia, Z.-J. Song, H. Xu, Y. Shi, L.-N. He, P. Cheng and B. Zhao, Angew. Chem., Int. Ed., 2020, 59, 8586–8593.

5 (a) M. Can, F. A. Armstrong and S. W. Ragsdale, Chem. Rev., 2014, 114, 4149–4174; (b) V. Waser, M. Mukherjee, R. Tachibana, N. V. Igareta and T. R. Ward, J. Am. Chem. Soc., 2023, 145, 14823–14830.

6 (a) F. Schwizer, Y. Okamoto, T. Heinisch, Y. Gu, M. M. Pellizzoni, V. Lebrun, R. Reuter, V. Köhler, J. C. Lewis and T. R. Ward, Chem. Rev., 2018, 118, 142–231; (b) E. N. Mirts, A. Bhagi-Damodaran and Y. Lu, Acc. Chem. Res., 2019, 52, 935–944.

7 (a) M. Zhao, H.-B. Wang, L.-N. Ji and Z.-W. Mao, Chem. Soc. Rev., 2013, 42, 8360–8375; (b) S. T. Stripp, B. R. Duffus, V. Fourmond, C. Léger, S. Leimkühler, S. Hirota, Y. Hu, A. Jasniewski, H. Ogata and M. W. Ribbe, Chem. Rev., 2022, 122, 11900–11973.

8 (a) H. Li, M. Eddaoudi, M. O'Keeffe and O. M. Yaghi, Nature, 1999, 402, 276–279; (b) H. Furukawa, K. E. Cordova, M. O'Keeffe and O. M. Yaghi, Science, 2013, 341, 1230444; (c) W. Xu, Y. Wu, W. Gu, D. Du, Y. Lin and C. Zhu, Chem. Soc. Rev., 2024, 53, 137–162; (d) K.-Y. Wang, J. Zhang, Y.-C. Hsu, H. Lin, Z. Han, J. Pang, Z. Yang, R.-R. Liang, W. Shi and H.-C. Zhou, Chem. Soc. Rev., 2023, 123, 5347–5420; (e) J. Liang, M. Y. B. Zulkifli, J. Yong, Z. Du, Z. Ao, A. Rawal, J. A. Scott, J. R. Harmer, J. Wang and K. Liang, J. Am. Chem. Soc., 2022, 144, 17865–17875; (f) J. Wu, Z. Wang, X. Jin, S. Zhang, T. Li, Y. Zhang, H. Xing, Y. Yu, H. Zhang, X. Gao and H. Wei, Adv. Mater., 2021, 33, 2005024; (g) S. Rojas-Buzo, P. Concepción, J. L. Olloqui-Sariego, M. Moliner and A. Corma, ACS Appl. Mater. Interfaces, 2021, 13, 31021–31030; (h) J. R. Bour, A. M. Wright, X. He and M. Dincă, Chem. Sci., 2020, 11, 1728–1737; (i) J. Chen, H. Gao, Z. Li, Y. Li and Q. Yuan, Chin. Chem. Lett., 2020, 31, 1398–1401; (j) Q. Sun, B. Aguila and S. Ma, Chem, 2018, 4, 2736–2738.

9 (a) G. T. Rochelle, Science, 2009, 325, 1652–1654; (b) T. M. McDonald, W. R. Lee, J. A. Mason, B. M. Wiers, C. S. Hong and J. R. Long, J. Am. Chem. Soc., 2012, 134, 7056–7065; (c) H. Lyu, O. I.-F. Chen, N. Hanikel, M. I. Hossain, R. W. Flaig, X. Pei, A. Amin, M. D. Doherty, R. K. Impastato, T. G. Glover, D. R. Moore and O. M. Yaghi, J. Am. Chem. Soc., 2022, 144, 2387–2396.

10 J. Li, L. He, Q. Liu, Y. Ren and H. Jiang, Nat. Commun., 2022, 13, 928.

11 (a) X. Feng, J. Hajek, H. S. Jena, G. Wang, S. K. P. Veerapandian, R. Morent, N. De Geyter, K. Leyssens, A. E. J. Hoffman, V. Meynen, et al, J. Am. Chem. Soc., 2020, 142, 3174–3183; (b) G. Fu, P. Wu, J. Yang, S. Zhang, L. Wang, M. Xu and X. Huai, Inorg. Chem., 2022, 61, 17943–17950.

12 (a) F. Yang, J. Wang, Y. Wang, B. Yu, Y. Cao, J. Li, L. Wu, J. Huang and Y.-N. Liu, Angew. Chem., Int. Ed., 2024, e202318115; (b) J. Li, J. Liao, Y. Ren, C. Liu, C. Yue, J. Lu and H. Jiang, Angew. Chem., Int. Ed., 2019, 58, 17148–17152.

13 M. C. Biesinger, L. W. M. Lau, A. R. Gerson and R. S. C. Smart, Appl. Surf. Sci., 2010, 257, 887–898.